Asymmetric supercapacitor based on novel coal fly ash derived metal–organic frameworks as positive electrode and its derived carbon as negative electrode

Khavharendwe Melba Rambau[1,2], Delvina Japhet Tarimo[2], Oladepo Fasakin[3], Nicholas Mulei Musyoka[1], Ncholu Manyala[2]

[1]Centre for Nanostructures and Advanced Materials (CeNAM), HySA Infrastructure Centre of Competence, Council for Scientific and Industrial Research (CSIR), Chemicals cluster, Pretoria, South Africa

[2]Department of Physics, Institute of Applied Materials, SARCHI Chair in Carbon Technology and Materials, University of Pretoria, Pretoria, South Africa

[3]Department of Physics and Engineering Physics, Obafemi Awolowo University, Ile-Ife, 220005, Nigeria

*Correspondence to Nicholas Mulei Musyoka. Email: NMusyoka@csir.co.za or
Ncholu Manyala. Email: ncholu.manyala@up.ac.za.

Abstract

The paper presents a comparative study between aluminum fumarate metal–organic framework (Al-FumMOF) and a novel coal fly ash derived aluminum MOF (CFA-FumMOF) with their respective MOF-derived carbons (MDCs) for electrochemical performance in supercapacitor application. In the half-cell configuration, Al-FumMOF possessed the highest specific capacity value of 28.62 mAh g^{-1} and CFA-FumMOF with 9.88 mAh g^{-1} at a specific current of 0.5 A g^{-1} in 6 M KOH electrolyte. The carbon derivative from CFA-FumMOF possessed the highest specific capacitance of 306.59 F g^{-1} at 0.5 A g^{-1} as compared to carbon obtained from Al-FumMOF (111.94 F g^{-1}). Each MOF was prepared with its respective carbon derivative for an asymmetrical capacitor device with a specific capacity of 5.09 mAh g^{-1} at 0.5 A g^{-1}.

Graphical abstract

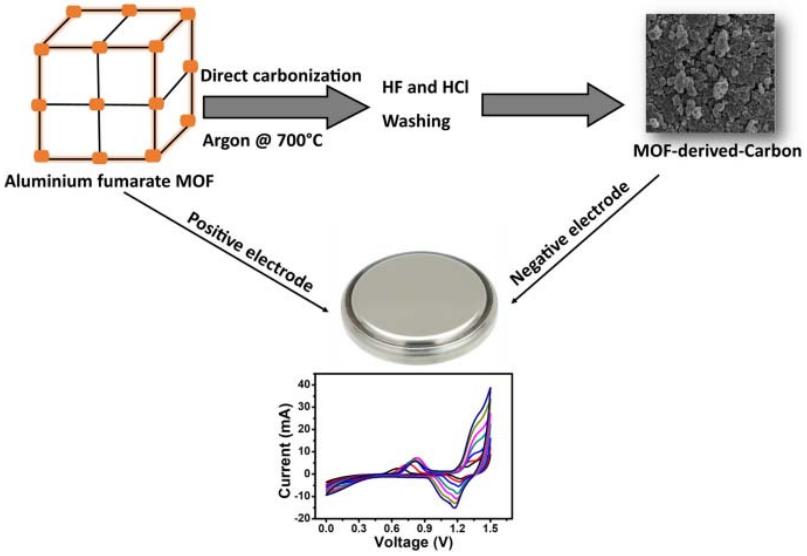

Keywords: Coal fly ash derived MOF; Aluminum fumarate MOF; MOF-derived Carbons; Asymmetric supercapacitor; Enhanced electrochemical performance

1 Introduction

Fossil fuels remain the dominant supplier of electrical energy worldwide [1]. Combustion of fossil fuel has proved to be cheap and reliable way for generating electricity. The approach has a drawback of being the single largest global greenhouse gas producer with an average of 1000 g lifecycle CO_2 emission per kWh of electricity [2,3,4]. For such a stance, the world has encountered social, political, and environmental strain to lower carbon emissions [5,6,7,8]. Many countries have endorsed regulations that involve industries with a high carbon footprint to acquire carbon allowances to regulate emissions and promote accountability. This has led many countries to enter a concord of Kyoto and Paris agreement that aims for the reduction of greenhouse gasses emitted by fossil fuels by 2060 [9, 10]. This would require a significant change in energy harnessing and a transition toward renewable energy (RE). The world energy outlook reported that for a global temperature rise to be limited to 2 °C by 2100, the world needs to attain carbon–neutral energy in which RE provides 60% of energy by the end of the century and 715 million electric vehicles utilized by 2040 [11,12,13]. This is a clear indication that the world is making a transition toward REs. Currently, many countries have amalgamated intermittent RE in their electrical power systems having benefits of improved power quality, voltage profile, stability, and reliability [14,15,16,17]. However, RE have minor drawbacks such as the unpredictable nature of the resources of RE, which gives a variable energy output with uncontrollable availability. The REs are also restricted and in most cases situated in a distance from load centers [18, 19]. Such REs are known as variable renewable energy sources (VRES), which are namely solar and wind [18, 20]. To resolve these issues, grid-compatible energy storage systems need to be developed, which consist of high capacity, high energy density, long-life cycle, reliability, and cost-effectiveness [11, 21]. Having energy storage systems enables efficient economic performances, load leveling, peak shaving, power quality improvement, and reliability [21]. Energy storage systems can be categorized as mechanical, chemical, thermal, electrical, and electrochemical [22,23,24]. Electrochemical is the most common and reliable energy storage systems, which includes Lithium-ion batteries (LIBs) and Supercapacitors (SCs) [25,26,27]. LIBs have a drawback in exhibiting high energy density, good rate performance, and low power density, whereas SCs have high-rate performance and low energy density [28]. Since the main drawback of developing SCs is energy density, it is paramount to find new materials that are cost effective and can improve the energy density [21]. There have been studies in the use of waste materials such as biomass, polyethylene plastic, and unconventional materials, which are converted to porous materials for SCs application [29,30,31]. Xu et al. reported on activated carbon from the apricot shell at 6 M KOH giving a high double layer capacitance of 339 F g^{-1} [32]. Rufford et al. reported on activated carbon from sugarcane bagasse giving a specific capacitance of 300 F g^{-1} [33]. Porous materials such as Metal Organic Frameworks (MOFs) have also been successfully applied and developed for SCs. MOFs are prepared by chemical coordination between metal and organic linkers to create an open crystalline framework with permanent porosity [34, 35]. Most have been used as electrodes materials providing acceptable electrochemical performance due to their tunable porosity. They can also be utilized as sacrificial templates to obtain metal oxides and highly porous carbons that can be used in SCs applications [36]. Metal oxides can be obtained through calcination under air whereas carbon materials can be obtained through wet impregnation or direct carbonization under an inert atmosphere. There are records of specific

capacitance as high as 232 F g^{-1} at 0.1 A g^{-1} of MOF-derived carbons [37]. In this study, the authors reported a comparative SCs study on the use of waste derived MOF, from coal fly ash (CFA-FumMOF), with structural properties similar to Aluminum fumarate MOF as candidates for electrode material. These materials undergo direct carbonization process to obtain MOF-derived carbons (MDCs) material. These MDCs are used as negative materials in an asymmetrical device in which their respective parent (MOFs) are the positive electrode. It is noteworthy to the reader that the morphological, structural, and textural properties of these materials have been discussed in a previous report [51] and this report will only cover the electrochemical performance of the materials. This communication covers the proof of concept in utilizing waste materials obtained from green synthesis of MOFs and derived carbons in the application of SCs.

2 Experimental

2.1 Material

Polyvinylidene fluoride (PVDF), Sulfuric acid (98%), and Hydrochloric acid (37%) were obtained from the Associated Chemical Enterprise (ACE) in South Africa. A deionized water was used for all the experiments. Argon (99%) was supplied from Afrox.

2.2 Preparation of activated carbon from cocoa

Preparation and characterization methods of CFA-FumMOF, Al-FumMOF and their carbon derivatives (CFA-MDC and Al-MDC) have been described in our previous report [51]. AC-Cocoa was prepared as follows: The cocoa pod husks (CPH) waste was collected from a dumping site in farmland and adopted as raw material. The CPH was repeatedly washed with acetone and distilled water to remove all the dirt and dried at 60 °C for 24 h in an electric oven. The cleaned and dried CPH was sliced into smaller pieces, 10 g of the sliced material was soaked in 100 mL of distilled water containing 10 mL of 0.5 M sulfuric acid and transferred into a 120 mL stainless steel autoclave unit which was then sealed and heated up at 160 °C for 12 h. The product was filtered and dried at 80 °C for another 48 h. The dried product was mixed together in an agate mortar with potassium hydroxide pellet in a mass ratio of 1:1 before being carefully placed in a horizontal tube furnace for carbonization at a ramping rate of 5 °C min^{-1} to 700 °C under a continuous flow of argon (300 sccm) for 60 min. Afterward, the carbonized material was washed with 3 M hydrochloric acid and distilled water until a neutral pH value was reached. The final product was dried at 60 °C for 24 h in an electric oven, producing activated carbon named AC-Cocoa.

2.3 Electrochemical investigation

Three and two-electrode configuration systems were used to conduct the electrochemical measurements. The electrodes were prepared by mixing 80% of the active material, 10% of conductive carbon acetylene black (CB), and 10% of Polyvinylidene fluoride (PVDF) as a binder and using a few drops of 1-methyl 2-pyrrolidone (NMP) to make a homogenous slurry. A clean nickel foam was used as a current collector and the slurry was pasted on an area of 1.0×1.0 cm^2 and dried at 60 °C for 12 h. Their capacitive performance was performed with the aid of a Bio-Logic VMP300 potentiostat (Knoxville TN 37,930, USA) controlled by EC-Lab V1.40 software in a three-electrode set-up. A glassy carbon was used as a counter electrode, Ag/AgCl as a reference electrode and working electrode consisting of the active material. The cyclic voltammetry (CV) of the as-prepared samples was performed at different

scan rates ranging from 5 to 100 mV s^{-1} at a potential window ranging from 0.0 to 0.4 V vs. Ag/AgCl. The galvanostatic charge–discharge (GCD) was performed at specific current range of 0.5 to 10 A g^{-1} at a potential window range of 0.0 to 0.4 V vs. Ag/AgCl. The specific capacity of a single electrode was calculated via a GCD profile using Eq. (1) below [50]

$$Q_s = \frac{I_d \times \Delta t}{3.6} \tag{1}$$

where Q_s is the specific capacity, I_d as specific current (A g^{-1}) and Δt is the discharge time (s). The specific capacitance Cs was calculated as follows [52]:

$$C_s = \frac{\Delta t \times I_d}{\Delta V} \tag{2}$$

With Δt as change in discharge time and ΔV is a potential difference. The coulombic efficiency (CE) was calculated using the equation below:

$$C_E = \frac{t_d}{t_c} \times 100\% \tag{3}$$

where t_c is the charging time and t_d is the discharging time.

The electrochemical impedance spectroscopy was measured using an open circuit potential of frequency range from 10 mHz—100 kHz. The asymmetric hybrid device was assembled using the as-prepared Al-fumMOF or CFA-FumMOF as a positive electrode and their respective MDCs (Al-MDC and CFA-MDC) as a negative electrode with a thickness and diameter of 0.2 and 16 mm, respectively, in a standard 2032 grade coin cell using Watman Celgard paper-based separator and 6 M KOH as electrolyte. The charge balance $Q_+ = Q_-$ was used to balance the mass of each electrode. The MOF materials exhibited Faradic behavior with specific capacity (Q_s) calculated by using the GCD curve as shown in Eq. (1) above. The charge balancing equation was written as follows [50]:

$$Q_+ = Q_- \rightarrow m_+ \times 3.6 Q_{s+} = m_- \times \Delta V_- \times C_{s-} \rightarrow \frac{m_-}{m_+} = \frac{3.6 \times Q_{s+}}{\Delta V_- \times C_{s-}} \tag{4}$$

where, Q_+ and Q_- is stored charge in positive and negative electrodes, respectively. Q_{s+} and C_{s-} are the specific capacity and capacitance for the positive and negative electrodes, respectively. $\Delta V\_$ is the potential window for the negative electrode and masses of the positive and negative electrodes are represented as m_+ and m_-, respectively. The prepared cell operated at a potential window of 0.0 to 1.5 V as influenced by the operating potential of the prepared electrodes. The specific capacity (Q_s) of the asymmetric device was calculated using Eq. (1).

The specific energy (E_d) and specific power (P_d) of the device were calculated as follows [50]:

$$E_d = \frac{1}{3.6m} \int V dt \tag{5}$$

$$P_d = \frac{E_d}{\Delta t} \times 3600 \tag{6}$$

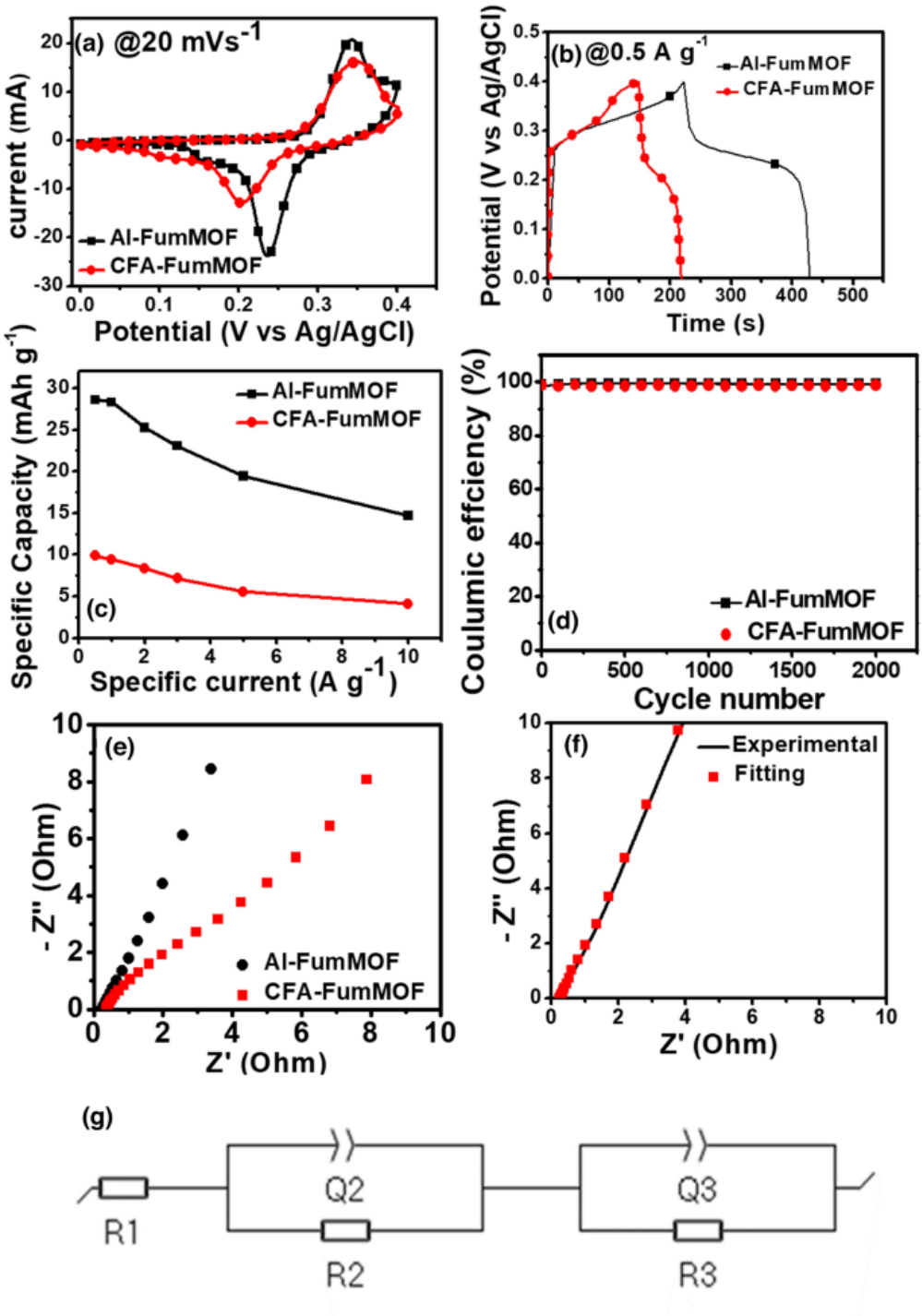

Fig. 1. a CV curves at a scan rate of 20 mV s-1. **b** GCD curves at a specific current of 0.5 A g-1. **c** Specific capacity against specific current. **d** Cycling performance. **e** EIS Nyquist plot for Al-FumMOF and CFA-FumMOF, respectively, in 6 M KOH in a positive potential window. **f, g** EIS Nyquist plot experimental and fitting, and its equivalent circuit for Al-FumMOF

3 Results and discussion

3.1 Three electrode measurements of prepared MOFs and their derived carbons

The electrochemical performance of the synthesized MOF materials was evaluated using a three-electrode configuration in 6 M KOH electrolyte. Figure 1a represents the cyclic voltammetry (CV) curves at a scan rate of 20 mV s^{-1} in the positive potential window range of 0.0 to 0.4 V vs. Ag/AgCl for Al-FumMOF and the novel CFA-FumMOF. The CV curves exhibit two redox peaks, which are attributed to the electrochemical redox reaction of the metallic Al (with numerous valence states) and the concentration of KOH electrolyte, which consists of the OH^- group with the highest ionic conductivity among anions. The depicted redox peaks from the CV curves are associated with the Faradic nature of the Al-FumMOF. The novel CFA-FumMOF also exhibited the Faradic behavior observed from the pristine material. The oxidation peaks were observed at 0.34 V and 0.35 V, and reduction peaks at 0.24 V and 0.20 V for Al-FumMOF and CFA-FumMOF, respectively. The galvanostatic charge/discharge (GCD) curves in Fig. 1b at a specific current of 0.5 A g^{-1} exhibit a non-linear curve with a potential plateau, which corresponds with the CV curves indicating battery-type SCs. By observation of both CV and GCD curves, it can be seen that the current response and discharge time of Al-FumMOF are higher than the novel CFA-FumMOF. This can be due to the presence of Fe^{3+} metal embedded within the CFA-FumMOF structure. Our group reported on the structural properties of CFA-FumMOF and speculated on the isomorphic substitution of Fe toward Al in the MOF structure [51]. It is expected that the presence of Fe would increase conductivity and stability as previous reports indicate [53, 54]; however, in this instance the opposite is true. The concept of bimetallic MOFs to enhance electrochemical performance relies on various principles: (i) quantity of the dopant or new metal introduced; (ii) the structural and morphological changes of the MOF after the introduction of the new metal; and (iii) synergy of the two metals within the structure [38,39,40,41].

Due to these reasons, there are no free holes created that improved the electrical conductivity instead, the Fe ion operates as in any Fe-based MOF, which has poor electrochemical performance. As a result, the presence of Fe ions inhibits the flow of electrons. Figure 1c depicts the specific capacity against specific current evaluated using Eq. (1) whereby both materials indicate good rate capability with a gradual decrease in specific capacity due to inability of the electrolyte ions to access the pores. Al-FumMOF possesses the highest specific capacity value of 28.62 mAh g^{-1} compared to that of CFA-FumMOF with 9.88 mAh g^{-1} at a specific current of 0.5 A g^{-1}. The electrochemical performance of Al-FumMOF and the novel CFA-FumMOF is relatively better when compared to other reported Al-based MOFs [46, 48, 49]. Previous reports on aluminum-based MOF known as MIL-53(Al) indicated the specific capacitance of 6.5 F g^{-1} at 0.5 A g^{-1}; this can also be attributed to its agglomerated morphology as opposed to the laminar structure possessed by both Al-FumMOF and CFA-FumMOF, which enables ease transportation of electrolyte ions. Figure 1d shows the coulombic efficiency for Al-FumMOF and CFA-FumMOF in 2000 cycles at 2 A g^{-1}. The half-cell configuration maintained efficiency of 99.31% for Al-FumMOF and 98.52% for CFA-FumMOF. Al-FumMOF has high cycling stability as compared to the novel CFA-FumMOF. It is also noteworthy that the synthesized MOFs in this paper are achieved through green chemistry as opposed to other Al-based MOFs. Figure 1e presents the EIS Nyquist plot of Al-FumMOF and CFA-FumMOF. It can be observed from the figure that Al-FumMOF exhibits a short diffusion length stipulating a fast charge transport as compared to CFA-FumMOF. The EIS was used to obtain Equivalent series resistance (ESR), which is the total resistance of the ionic resistance of the electrolyte, the electrolyte/electrode interface resistance and electrode/current collector

interface resistance [52]. The ESR values were obtained from Z ' axis intersect and are 0.21 Ω and 0.44 Ω for Al-FumMOF and CFA-FumMOF, respectively. The ESR value of Al-FumMOF corroborates the good electrochemical performance as compared to CFA-FumMOF. The charge transfer resistance (R_{ct}) is associated with the charge transfer between the interfaces and was obtained from the semi-circle at high-frequency region with the values of 0.08 and 0.12 for Al-FumMOF and CFA-FumMOF, respectively. The EIS Nyquist plot of Al-FumMOF was fitted with the circuit presented in Fig. 1g.The ESR value from the circuit is represented by R1 at a high-frequency region with charge transfer resistance (R_{ct}) represented by R2. R3 is associated with leakage resistance (R_l), with Q2 and Q3 associated with real capacity. The fitted ESR value is 0.28 Ω and R_{ct} value is 0.10 Ω, which corresponds to experimental values. The MOF-derived carbons (MDCs) were also analyzed for their electrochemical properties using a three-electrode configuration in 6 M KOH in a negative potential window range of -1.0 to 0.0 V vs. Ag/AgCl.

Figure 2a shows the comparative CV curves of Al-MDC and CFA-MDC, which suggest EDLC behavior corroborated with the relatively rectangular shape of the curve. It can also be observed that the CFA-FumMOF consisted of the longest discharge time compared to Al-MDC at 0.5 A g^{-1}, indicating better electrochemical performance (Fig. 2b). Generally, the electrochemical performance of carbon materials is dependent on its surface area. The surface area of both carbons are relatively the same (2438 m^2 g^{-1} for Al-MDC and 2017 m^2 g^{-1} for CFA-MDC) [51]. However, CFA-MDC appears to have high specific capacitance of 306.59 F g^{-1} at 0.5 A g^{-1} as compared to Al-MDC with the value of 111.94 F g^{-1} as evaluated using Eq. (2). These values are consistent with other reports of MOF-derived carbons from aluminum-based MOFs. Zhang et al. reported on MDC obtained from MIL-53(Al) giving a specific capacitance of 298 F g^{-1} at 1 mV s^{-1} in 1 M H_2SO_4 [42]. Yan et al. reported on MDC from Al(OH)(1.4-NDC)0.2H_2O, which reached a specific capacitance of 232.8 F g^{-1} at a specific current of 0.1 A g^{-1} [37]. Also, the specific capacitance of the MDCs may differ due to the pore sizes of the parent MOFs. On the other hand, the metal node (Al) maybe similar, but the porous structure of the MOF may differ due to the organic linkers used for coordination, which result in similar MOFs with different pore sizes and as a result, the MDCs porous structure may differ. The as-prepared carbons (Al-MDC and CFA-MDC) had the presence of narrower polymodal micropore distribution centered at 1.2 nm and 1.5 nm with CFA-MDC possessing wider mesopores. The mesoporous structure enabled free and easy access of electrolyte ions [5]. The GCD curve in Fig. 2b for CFA-MDC also assume a near symmetrical triangular shape associated with good columbic efficiency as depicted in Fig. 2d. CFA-MDC has columbic efficiency of 99.62% and Al-MDC of 98.79% indicating good cyclability. Figure 2e represents the EIS Nyquist plot of Al-MDC and CFA-MDC. CFA-MDC is exhibiting short diffusion length which already corresponds to the specific capacitance. The experimental ESR values were 1.16 Ω and 0.26 Ω for Al-MDC and CFA-MDC, respectively. The small ESR value of CFA-MDC is associated with good wettability. The fitting of CFA-MDC is depicted in Fig. 2f with the circuit in Fig. 2g. The ESR value is represented by R1 and charge transfer resistance (R_{Ct}) represented by R2, leakage resistance (R_l) is represented by R3 and R4, with Q2 and Q3 associated with real capacity. From the fitting of CFA-MDC, the ESR value is 0.31 Ω and R_{ct} value is 0.27 Ω, which corresponds well to the experimental values of 0.38 and 0.24 Ω, respectively. The small R_{ct} values indicates good charge transfer kinetics and hence reflect the performance observed for CFA-MDC electrode. This explain the linked attribute of CFA-MDC as a capacitive material [52].

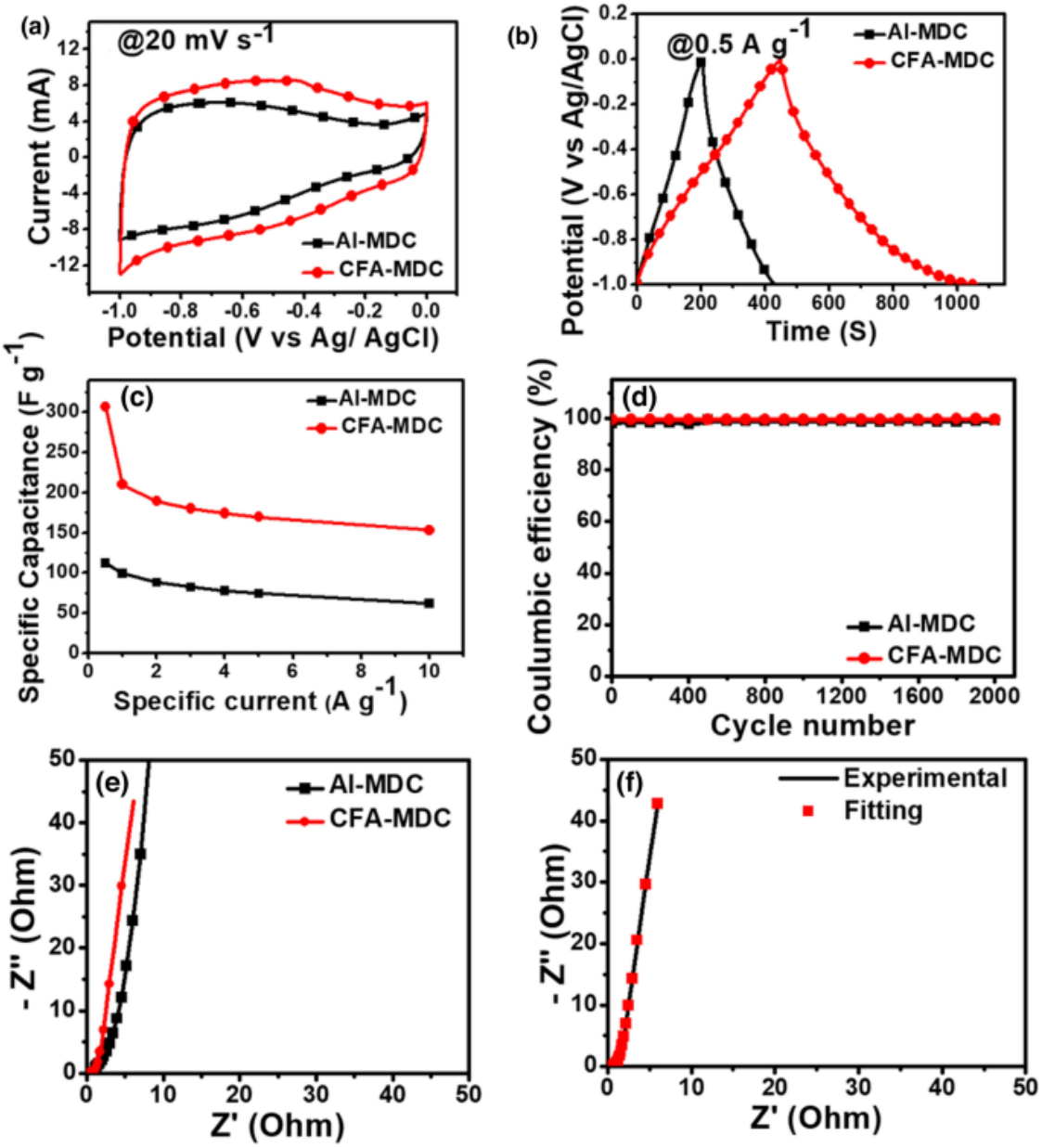

Fig. 2. a CV curves at a scan rate of 20 mV s-1. **b** GCD curves at a specific current of 0.5 A g-1. **c** Specific capacitance against specific current. **d** Cycling performance. **e** EIS Nyquist plot for Al-MDC and CFA-MDC, respectively, in 6 M KOH in a negative potential window. **f, g** EIS Nyquist plot experimental and fitting, and its equivalent circuit for CFA-MDC

The prepared MOFs were used as the positive electrode and their respective carbon derivatives were used as a negative electrode for a full cell device. The asymmetric device of Al-FumMOF//Al-MDC was assembled with mass balancing using Eq. (4) giving a ratio of 3.0:1.0 and working with a total mass electrode of 7.1 mg cm^{-2}. The assembly was done with a standard 2032 grade coin cell sandwiched with a filter paper as separator and 6 M KOH as electrolyte. Figure 3a displays the CV curve at a scan rate of 40 mV s^{-1} of Al-FumMOF at a positive potential window of 0.0–0.4 V vs. Ag/AgCl and Al-MDC at a negative potential window of -1.0–0.0 V vs. Ag/AgCl. The curve gives an illustration of EDLC and Faradic behavior, with EDLC contribution visible in both positive and negative currents; however,

Faradic contributions show dominance with a much higher positive current. Subsequently, the combination of the two responses is expected to create a battery-like behavior in the device. The CV curves of the device are represented in Fig. 3b at different scan rates of 5 to 100 mV s^{-1}. The curves illustrate a merger between EDLC and Faradic contribution associated with hybrid asymmetric supercapacitors. The GCD curves at different specific currents ranging from 0.5 to 10 A g^{-1} are depicted in Fig. 3c and show the potential steps confirming the Faradic behavior from the CV curves. As a result, the specific capacity of the device was calculated using Eq. (1) obtaining a value of 5.09 mAh g^{-1} at a specific current of 0.5 A g^{-1} (Fig. 3d). The capacities dropped as the specific current increased due to the limited ion migration associated with diffusion on the outer surface of the material for charge storage at a higher specific current [43]. It can be observed that there is a drop from the specific capacities in the device as compared to the three-electrode system, which is due to an increase in an electronic field in the cell configuration working at a high potential window, which is subsequently increased by the increase in specific current. This result in an overall interruption in the collaboration of Faradic and EDLC processes [44]. The specific energy and power of the device evaluated using Eq. (5) and Eq. (6) at 1 A g^{-1} was 10.12 Wh kg^{-1} and 552.09 W kg^{-1}, respectively. This is expected as an indication of low specific capacity. Figure 3e illustrates the coulombic efficiency of 99.10%, indicating good cyclability after 5000 cycles. Figure 3f illustrates the Nyquist plot showing fitting and experimental data. The circuit (Fig. 3h) consists of R1, R2, and R3 that represent equivalent series resistance (ESR), charge transfer resistance (R_{ct}) and leakage resistance, respectively. Q2 and Q3 are associated with real capacity and with the Warburg (W) element in series with the circuit. R2 and Q2 is associated with the resistance rate and Faradaic electrochemical activity occurring between the electrode and electrolyte. The experimental ESR values are 3.00 Ω and 3.06 Ω and R_{ct} values are 0.64 Ω and 1.69 Ω for before and after cycling stability. The values correspond with the fitted ESR value of 3.14 Ω and 3.17 Ω with R_{ct} values of 0.99 Ω and 1.23 Ω. It is noteworthy that the R_{ct} value before cycling is small compared to after cycling. This indicates that the material becomes more resistive after 5000 cycles and hence gives poor performance.

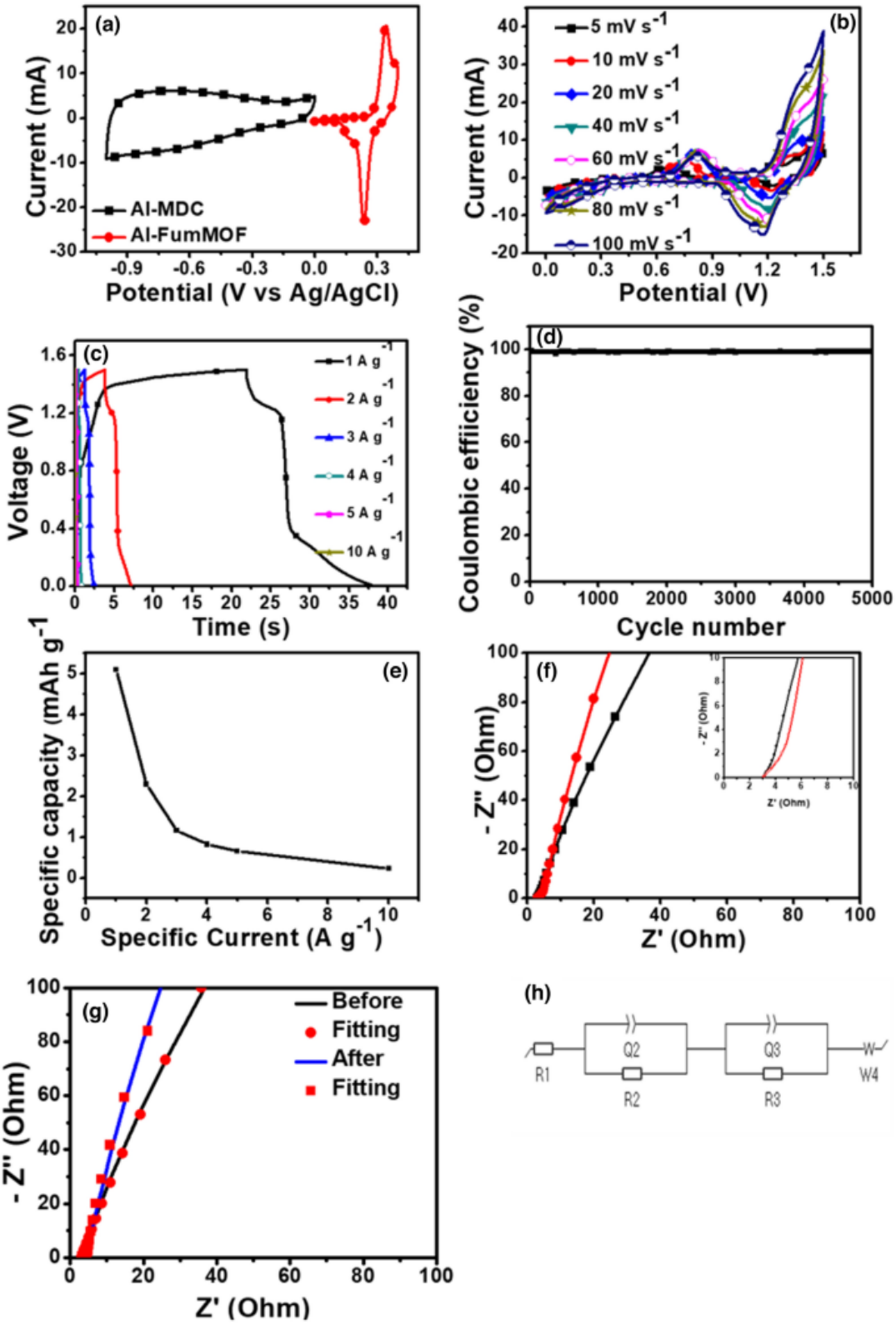

Fig. 3. Al-FumMOF//Al-MDC asymmetric device: **a** CV of positive and negative electrodes at scan rate of 20 mV s-1. **b** CV curves at different scan rates. **c** GCD curves at different specific currents. **d** Specific capacity versus specific current. **e** Cycling stability versus cycle number for the device. **f, g** EIS Nyquist plot and Fitting of EIS Nyquist plot before and after cycling and (h) Equivalent circuit from the fitting

The asymmetric device of CFA-FumMOF//CFA-MDC was assembled with mass balancing using Eq. (5) giving a ratio of 5.0:1.0 and working with a total mass electrode of 6.8 mg cm^{-2}. The cell was assembled under the same conditions mentioned prior. Figure 4a is illustrating the CV curves for CFA-FumMOF in the potential window of 0.0–0.4 V vs. Ag/AgCl and CFA-MDC at -1.0–0.0 V vs. Ag/AgCl. The CFA-FumMOF electrode shows the Faradic behavior corroborated by redox peaks with CFA-MDC demonstrating the pseudocapacitive behavior demonstrated by a relatively rectangular shape, indicating a reversible capacitive behavior [45,46,47]. The CV curves of the asymmetrical device of CFA-FumMOF//CFA-MDC are shown in Fig. 4b at scan rates from 5 to 100 mV s^{-1}. The curves illustrate the non-linear pseudocapacitive behavior, which operated from a potential window of 0.0–1.45 V. The GCD profiles represented by Fig. 4c at different specific currents from 0.5 to 10 A g^{-1} illustrates a quasi-linear curve with Faradic contribution, which corresponds well to the CV curves. The specific capacity recorded is 4.0 mAh g-1 at 0.5 A g^{-1} (Fig. 4d). The device obtained a good coulombic efficiency of 98.90% after 5000 cycles as depicted in Fig. 4e. The specific energy and power of the device calculated using Eq. (5) and Eq. (6) at 1 A g^{-1} are 2.48 Wh kg^{-1} and 625 W kg^{-1}, respectively. There are no known reports on the use of pristine aluminum-based MOF as a supercapacitor device. However, there is a single report on the use of an optimized aluminum MOF, which is involved the integration of the MOF structure with reduced graphene oxide (rGO) [46]. This study reported the energy density of 6.66 Wh kg^{-1} and power density of 3655 W kg^{-1}. The rGO assisted in reducing agglomeration of the MOF creating more active sites interacting with electrolytes and increasing charge storage. It can therefore be stipulated that an optimization process of CFA-FumMOF and Al-FumMOF could yield an improved electrochemical performance and energy density. In three-electrode configurations, the prepared MOFs illustrated a faradic behavior and their derived carbons illustrated a typical EDLC behavior as expected. Their electrochemical performance was relatively improved as compared to other reported aluminum-based MOFs [46, 48, 49]. Therefore, the specific capacity and capacitance reported herein are the highest in record.

3.2 Asymmetric supercapacitor device MOFs and activated carbon from cocoa

However, on the electrochemical device there is poor performance and to observe the compatibility of the prepared MOFs with other carbon materials, an asymmetrical device with the MOFs as a positive electrode and activated carbon from cocoa as a negative electrode was fabricated. The activated carbon possessed obvious EDLC behavior with a specific capacitance of 123.78 F g^{-1} at 0.5 A g^{-1} as shown in Fig. 5. Both Al-FumMOF//AC-Cocoa and CFA-FumMOF//AC-Cocoa devices had a potential window of 0.0 to 1.5 V and exhibited battery-type behavior corroborated with redox peaks. Al-FumMOF//AC-Cocoa possessed a specific capacity of 5.02 mAh g^{-1} and CFA-FumMOF possessed 4.74 mAh g^{-1} as presented in Figs. 6 and 7, respectively. Despite the change in the negative electrode, the devices did not improve in performance. Al-FumMOF//AC-Cocoa had coulombic efficiency of 99.00% and 98.23% for CFA-FumMOF//AC-Cocoa indicating good cyclability after 5000 cycles. This is an indication that both Al-FumMOF and CFA-FumMOF struggle with synergy with a negative electrode. The prepared asymmetric devices did not exhibit good electrochemical performance in practical instances. It is noteworthy to the reader that there are no known reports on the utilization of aluminum fumarate MOF (Al-FumMOF) as a positive electrode for the use of SCs. In addition, CFA-FumMOF is a novel MOF obtained through green synthesis and was prepared as a mimic of aluminum fumarate MOF as means of cutting costs in MOF synthesis industry. This study is a proof of concept on the use of green prepared materials for SCs application. The improved performance of the three-electrode measurements of the MOFs shows that if optimization processes such as preparing a composite are achieved, the materials

have the potential to outperform the most known MOF. With different activated carbon materials utilized as negative electrodes, the device can also have improved energy and power density.

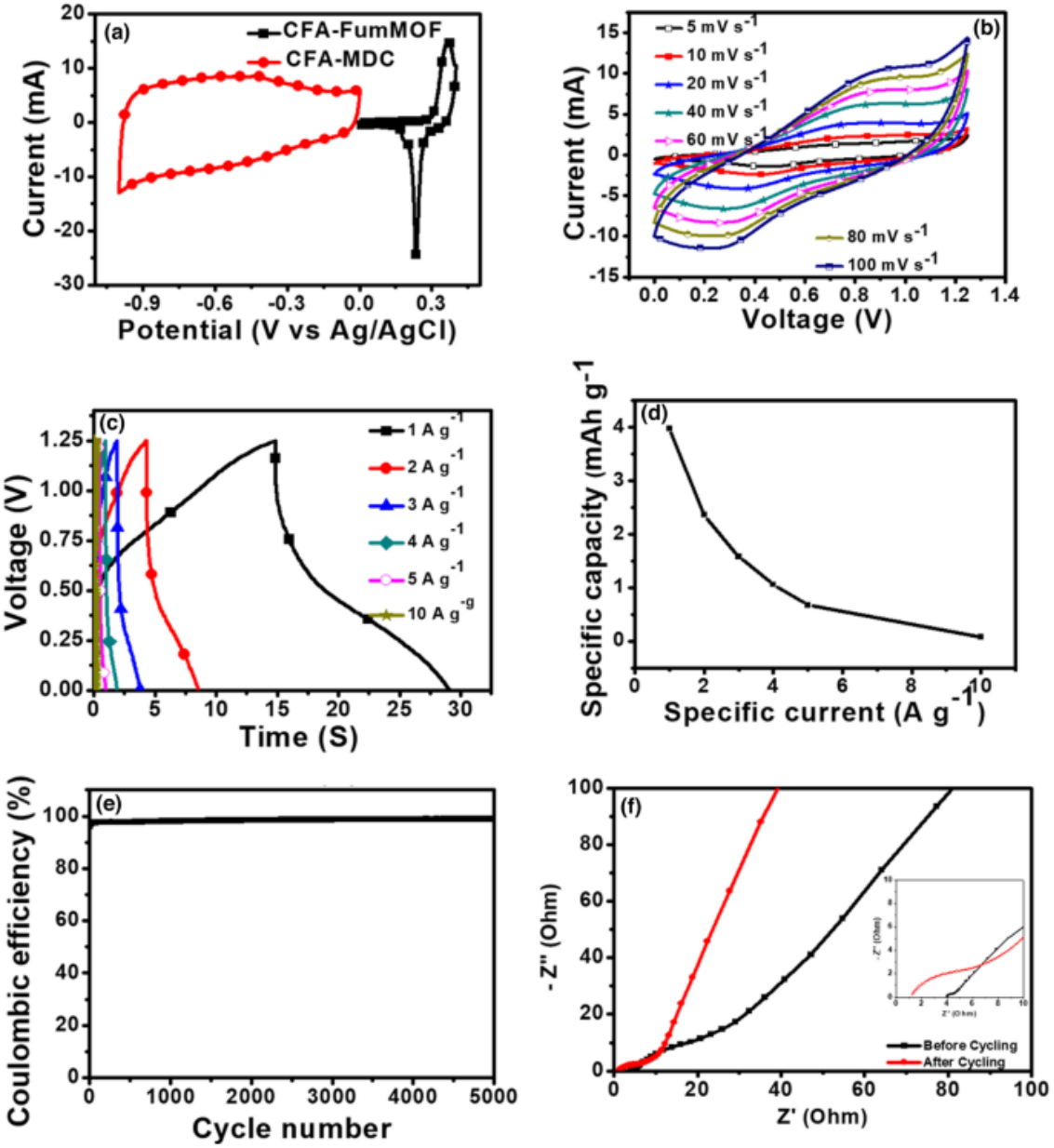

Fig. 4. CFA-FumMOF//CFA-MDC asymmetric device: **a** CV of positive and negative electrodes at scan rate 20 mV s-1. **b** CV curves at different scan rates. **c** GCD curves at different specific currents. **d** Specific capacity versus specific current. **e** Cycling stability versus cycle number for the device. **f** EIS Nyquist plot before and after cycling

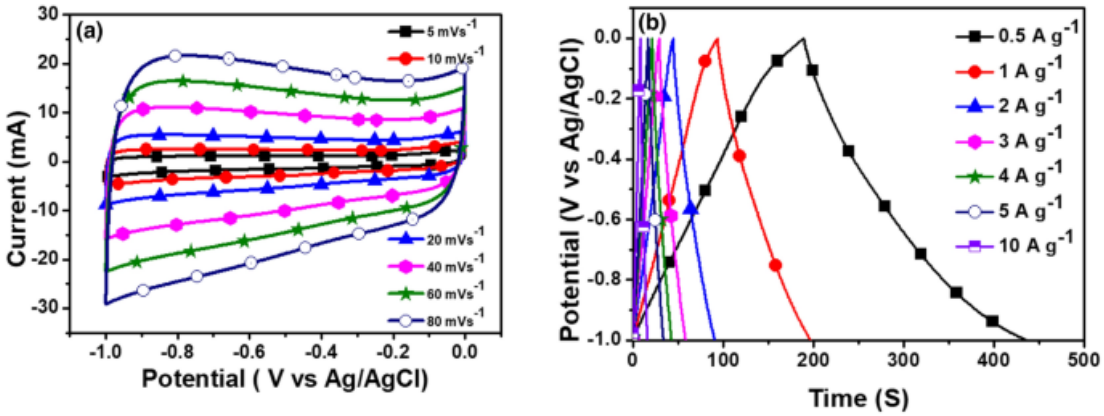

Fig. 5. a CV curves at different scan rates and **b** GCD curves at different specific currents for AC-Cocoa in 6 M KOH in a negative potential window

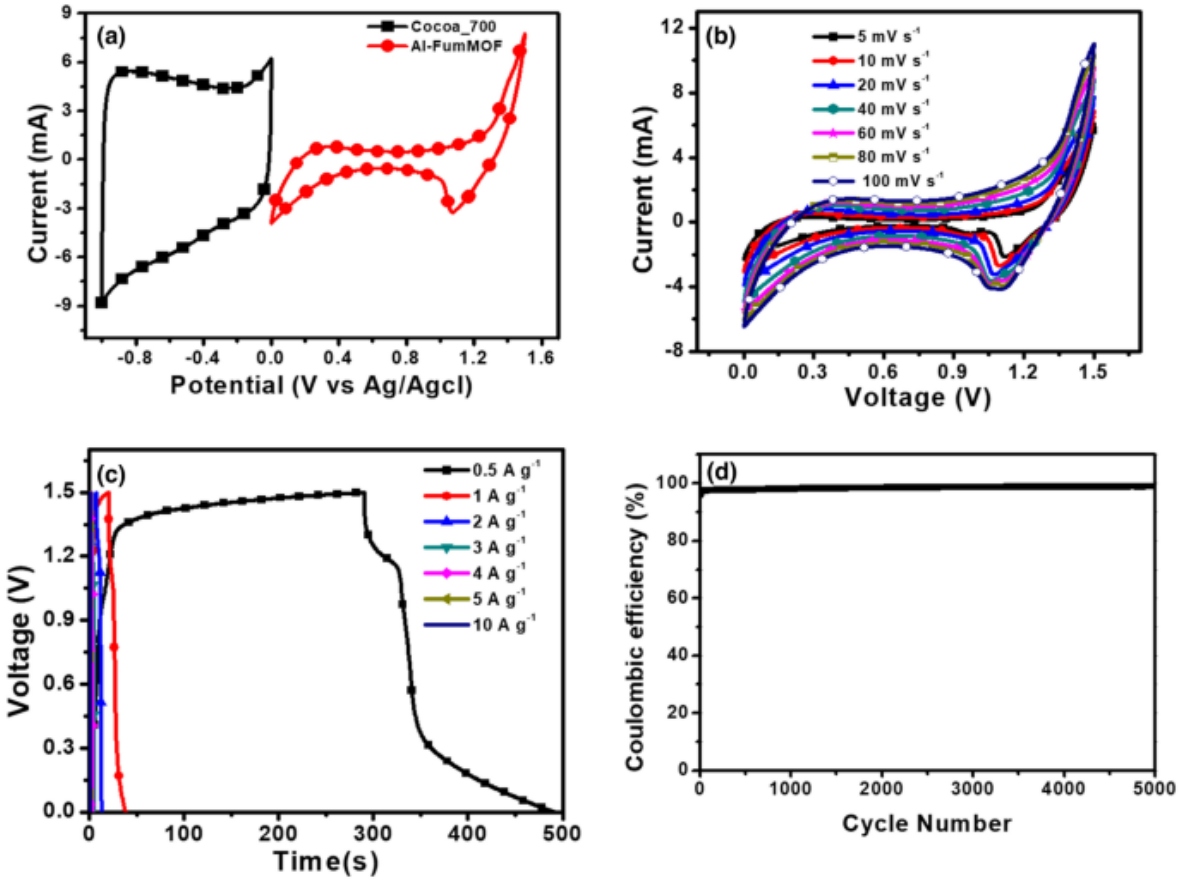

Fig. 6. Al-FumMOF//AC-Cocoa asymmetric device: **a** CV curve of positive and negative electrodes at 20 mV s-1 scan rate. **b** CV curves at different scan rates. **c** GCD curves at different specific currents. **d** Cycling stability versus cycle number

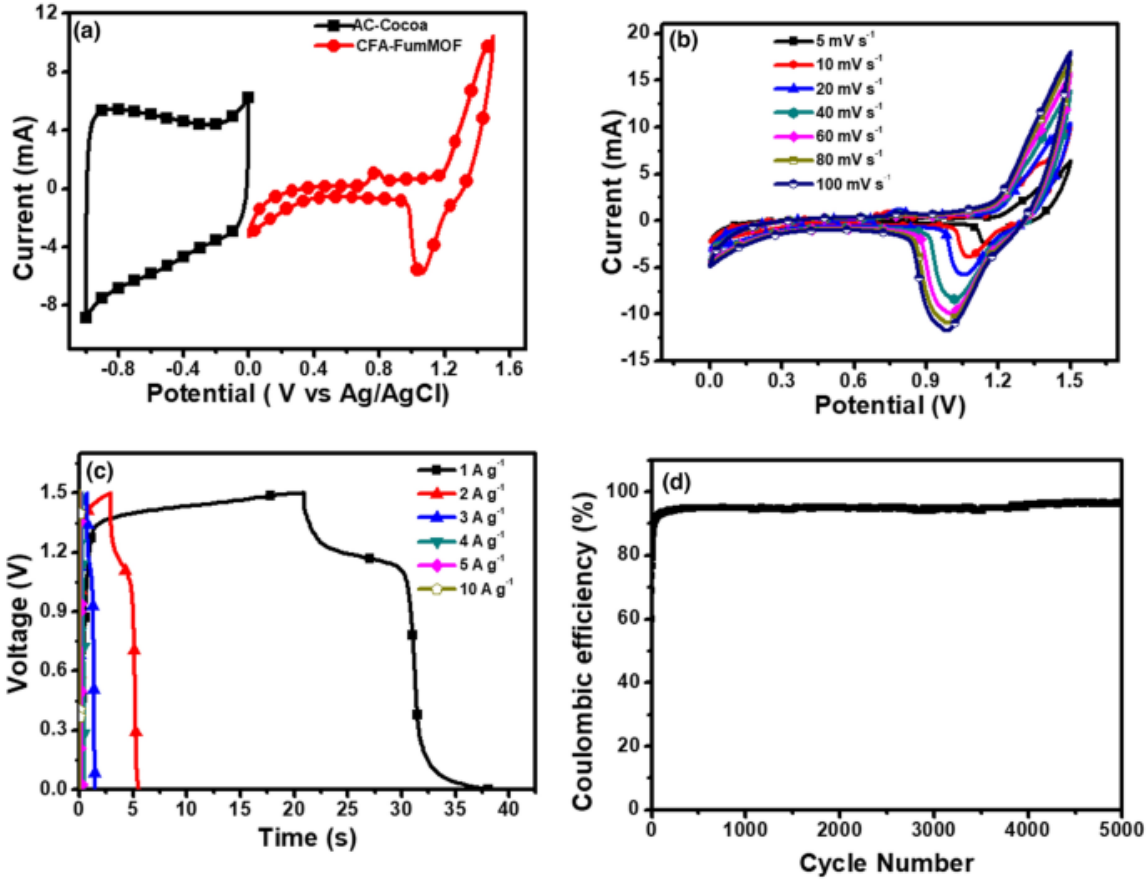

Fig. 7. CFA-FumMOF//AC-Cocoa asymmetric device: **a** CV of positive and negative electrodes at scan rate20 mV s-1. **b** CV curves at different scan rates. **c** GCD curves at different specific currents. **d** Cycling stability versus cycle number

4 Conclusion

The three-electrode measurements of Al-FumMOF and novel CFA-FumMOF were successfully prepared with a specific capacity of 28.62 mAh g^{-1} and 9.88 mAh g^{-1}, respectively, at a specific current of 0.5 A g^{-1}. Their respective MDCs, Al-MDC and CFA-MDC obtained a specific capacitance of 111.94 F g^{-1} and 306.59 F g^{-1}, respectively, at 0.5 A g^{-1}. There are no known records on the use Al-FumMOF as an electrode or on carbonization in attempts to obtain, a porous carbon used as a negative electrode in SCs. The asymmetric device did not provide good electrochemical performance. However, this study still serves as an entry point in the utilization of cheap waste materials to obtain exceptional MOF materials that can in turn be used as parent materials to obtain porous carbons and used for SCs application. The high surface area and exceptional porosity of the MOFs and their carbon derivative enables them to be used also in other energy storage applications.

Acknowledgements

KR would like to acknowledge the financial support from the South African Department of Science and Innovation (DSI) for research activities under the HySA Infrastructure as well as the National Research Foundation (NRF). KR also acknowledges the financial support by South African Research Chairs Initiatives (SARChI) of the Department of Science and

Technology and the National Research Foundation (NRF) of South Africa (Grant No. 61056). Any opinions, findings and/or recommendations expressed here are those of the authors and not of the funding bodies.

Contributions

KMR: Investigation, Methodology, Writing—original draft, Visualization. NM: Conceptualization, Supervision, Funding acquisition, Writing—review & editing. DJT: Methodology, Writing—review & editing. OF: Methodology, NM: Supervision, Writing—review & editing.

Conflict of interest

The authors declare that they have no conflict of interest.

References

1. DJ Wuebbles AK Jain 2001 Concerns about climate change and the role of fossil fuel use Fuel Process Technol 71 1–3 99 119
2. T Kåberger 2018 Progress of renewable electricity replacing fossil fuels Glob energy interconnect 1 1 48 52
3. Z Yang J Zhang MCW Kintner-Meyer X Lu D Choi JP Lemmon J Liu 2011 Electrochemical energy storage for green grid Chem Rev 111 5 3577 3613
4. F Martins C Felgueiras M Smitkovág 2018 Fossil fuel energy consumption in European countries Energy Procedia 153 107 111
5. Ü Ağbulut S Sarıdemir 2019 A general view to converting fossil fuels to cleaner energy source by adding nanoparticles Int J Ambient Energy 2019 1 6
6. SD Musa T Zhonghua AO Ibrahim M Habib 2018 China's energy status: a critical look at fossils and renewable options Renew Sustain Energy Rev 81 2281 2290
7. A Cornelius R Bandyopadhyay D Patiño-Echeverri 2018 Assessing environmental, economic, and reliability impacts of flexible ramp products in MISO's electricity market Renew Sustain Energy Rev 81 2291 2298
8. N Khan S Dilshad R Khalid AR Kalair N Abas 2019 Review of energy storage and transportation of energy Energy Storage 1 3 e49
9. D Held C Roger 2018 Three models of global climate governance: from Kyoto to Paris and beyond Global Pol 9 4 527 537
10. JH Krug 2018 Accounting of GHG emissions and removals from forest management: a long road from Kyoto to Paris Carbon Balance Manag 13 1 11
11. TM Gür 2018 Review of electrical energy storage technologies, materials and systems: challenges and prospects for large-scale grid storage Energy Environ Sci 11 10 2696 2767
12. M Salvia D Reckien F Pietrapertosa P Eckersley NA Spyridaki A Krook-Riekkola O Heidrich 2021 Will climate mitigation ambitions lead to carbon neutrality? An analysis of the local-level plans of 327 cities in the EU Renew Sustain Energy Rev 135 e110253
13. V Ramanathan J Allison M Auffhammer D Auston AD Barnosky L Chiang J Christensen 2016 Bending the curve: ten scalable solutions for carbon neutrality and climate stability Collabra 2 1 1 15
14. DO Akinyele RK Rayudu 2014 Review of energy storage technologies for sustainable power networks Sustain Energy Technol 8 74 91

15. JP Barton DG Infield 2004 Energy storage and its use with intermittent renewable energy IEEE Trans Energy Convers 19 2 441 448
16. A Henriot 2015 Economic curtailment of intermittent renewable energy sources Energy Econ 49 370 379
17. H Zsiborács NH Baranyai A Vincze L Zentkó Z Birkner K Máté G Pintér 2019 Intermittent renewable energy sources: the role of energy storage in the european power system of 2040 Electronics 8 7 729
18. AB Gallo JR Simões-Moreira HKM Costa MM Santos EM Santos Dos 2016 Energy storage in the energy transition context: a technology review Renew Sustain Energy Rev 65 800 822
19. G Notton ML Nivet C Voyant C Paoli C Darras F Motte A Fouilloy 2018 Intermittent and stochastic character of renewable energy sources: consequences, cost of intermittence and benefit of forecasting Renew Sustain Energy Rev 87 96 105
20. KP Kampouris V Drosou C Karytsas M Karagiorgas 2020 Energy storage systems review and case study in the residential sector Earth Environ Sci 410 1 e012033
21. S Koohi-Fayegh MA Rosen 2020 A review of energy storage types, applications and recent developments J Energy Storage 27 e101047
22. AG Olabi C Onumaegbu T Wilberforce M Ramadan MA Abdelkareem Al–Alami AH, 2020 Critical review of energy storage systems Energy 214 e118987
23. MS Guney Y Tepe 2017 Classification and assessment of energy storage systems Renew Sustain Energy Rev 75 1187 1197
24. M Faisal MA Hannan PJ Ker A Hussain MB Mansor F Blaabjerg 2018 Review of energy storage system technologies in microgrid applications: Issues and challenges Ieee Access 6 35143 35164
25. L Chang W Zhang S Xu K Spence 2017 Review on distributed energy storage systems for utility applications IEEE Trans Power Electron 2 4 267 276
26. L Zhang X Hu Z Wang J Ruan C Ma Z Song MG Pecht 2020 Hybrid electrochemical energy storage systems: an overview for smart grid and electrified vehicle applications Renew Sustain Energy Rev 139 e110581
27. GZ Chen 2017 Supercapacitor and supercapattery as emerging electrochemical energy stores Int Mater Rev 62 4 173 202
28. X Gao Y Dong S Li J Zhou L Wang B Wang 2020 MOFs and COFs for batteries and supercapacitors EER 3 1 81 126
29. M Fu W Chen J Ding X Zhu Q Liu 2019 Biomass waste derived multi-hierarchical porous carbon combined with $CoFe_2O_4$ as advanced electrode materials for supercapacitors J Alloys Compd 782 952 960
30. C Ma J Min J Gong X Liu X Mu X Chen T Tang 2020 Transforming polystyrene waste into 3D hierarchically porous carbon for high-performance supercapacitors Chemosphere 253 e126755
31. L Li C Jia X Zhu S Zhang 2020 Utilization of cigarette butt waste as functional carbon precursor for supercapacitors and adsorbents J Clean Prod 256 e120326
32. B Xu Y Chen G Wei G Cao H Zhang Y Yang 2010 Activated carbon with high capacitance prepared by NaOH activation for supercapacitors Mater Chem Phys 124 1 504 509
33. TE Rufford D Hulicova-Jurcakova K Khosla Z Zhu GQ Lu 2010 Microstructure and electrochemical double-layer capacitance of carbon electrodes prepared by zinc chloride activation of sugar cane bagasse J Power Sources 195 3 912 918
34. U Mueller M Schubert F Teich H Puetter K Schierle-Arndt J Pastre 2006 Metal–organic frameworks—prospective industrial applications J Mater Chem 16 7 626 636

35. H Li M Eddaoudi M O'Keeffe OM Yaghi 1999 Design and synthesis of an exceptionally stable and highly porous metal-organic framework Nature 402 6759 276 279
36. Y Zhao J Liu M Horn N Motta M Hu Y Li 2018 Recent advancements in metal organic framework based electrodes for supercapacitors Sci China Mater 61 2 159 184
37. X Yan X Li Z Yan S Komarneni 2014 Porous carbons prepared by direct carbonization of MOFs for supercapacitors Appl Surf Sci 308 306 310
38. MS Rahmanifar H Hesari A Noori MY Masoomi A Morsali MF Mousavi 2018 A dual Ni/Co-MOF-reduced graphene oxide nanocomposite as a high performance supercapacitor electrode material Electrochim Acta 275 76 86
39. D Zheng H Wen X Sun X Guan J Zhang W Tian Y Yao 2020 Ultrathin Mn doped Ni-MOF nanosheet array for highly capacitive and stable asymmetric supercapacitor Chem Eur J 26 71 17149 17155
40. F Jeremias A Khutia SK Henninger C Janiak 2012 MIL-100 (Al, Fe) as water adsorbents for heat transformation purposes—a promising application J Mater Chem 22 20 10148 10151
41. J Wang Q Zhong Y Xiong D Cheng Y Zeng Y Bu 2019 Fabrication of 3D Co-doped Ni-based MOF hierarchical micro-flowers as a high-performance electrode material for supercapacitors Appl Surf Sci 483 1158 1165
42. S Zhang X Shi D Moszyński T Tang PK Chu X Chen E Mijowska 2018 Hierarchical porous carbon materials from nanosized metal-organic complex for high-performance symmetrical supercapacitor Electrochim Acta 269 580 589
43. DY Momodu F Barzegar A Bello J Dangbegnon T Masikhwa J Madito N Manyala 2015 Simonkolleite-graphene foam composites and their superior electrochemical performance Electrochim Acta 151 591 598
44. TM Masikhwa F Barzegar JK Dangbegnon A Bello MJ Madito D Momodu N Manyala 2016 Asymmetric supercapacitor based on VS_2 nanosheets and activated carbon materials RSC Adv 6 45 38990 39000
45. MS Rahmanifar H Hesari A Noor MY Masoomi A Morsali MF Mousavi 2018 A dual Ni/Co-MOF-reduced graphene oxide nanocomposite as a high performance supercapacitor electrode material Electrochim Acta 275 76 86
46. M Majumder RB Choudhary AK Thakur A Khodayari M Amiri R Boukherroub S Szunerits 2020 Aluminum based metal-organic framework integrated with reduced graphene oxide for improved supercapacitive performance Electrochim Acta 353 e136609
47. T Wu N Prasetya K Li 2020 Recent advances in aluminium-based metal-organic frameworks (MOF) and its membrane applications J Membr Sci 6 e118493
48. H He G Wang B Shen Y Wang Z Lu S Guo Z Xiao 2020 Three isostructural Zn/Ni nitro-containing metal-organic frameworks for supercapacitor J Solid State Chem 288 e121375
49. Y Gong J Li PG Jiang QF Li JH Lin 2013 Novel metal (II) coordination polymers based on N, N′-bis-(4-pyridyl) phthalamide as supercapacitor electrode materials in an aqueous electrolyte Dalton Trans 42 5 1603 1611
50. DJ Tarimo KO Oyedotun AA Mirghni B Mutuma NF Sylla P Murovhi N Manyala 2020 Enhanced electrochemical performance of supercapattery derived from sulphur-reduced graphene oxide/cobalt oxide composite and activated carbon from peanut shells Int J Hydrog Energy 45 58 33059 33075
51. KM Rambau NM Musyoka R Panek W Franus M Wdowin N Manyala 2021 Preparation of coal fly ash derived metal organic frameworks and their carbon derivatives Mater Today Commun 27 e102433

52. DJ Tarimo KO Oyedotun AA Mirghni NF Sylla N Manyala 2020 High energy and excellent stability asymmetric supercapacitor derived from sulphur-reduced graphene oxide/manganese dioxide composite and activated carbon from peanut shell Electrochim Acta 353 e136498
53. H Yu H Xia J Zhang J He S Guo Q Xu 2018 Fabrication of Fe-doped Co-MOF with mesoporous structure for the optimization of supercapacitor performances Chin Chem Lett 29 6 834 836
54. L Liu Y Yan Z Cai S Lin X Hu 2018 Growth-oriented Fe-based MOFs synergized with graphene aerogels for high-performance supercapacitors Adv Mater Interfaces 5 8 1701548